Available online at www.sciencedirect.com
SCIENCE DIRECT®
Journal of Power Sources 119–121 (2003) 690–694
JOURNAL OF POWER SOURCES
www.elsevier.com/locate/jpowsour

Improvement of electrode performances of spinel $LiMn_2O_4$ prepared by mechanical alloying and subsequent firing

Woon Tae Jeong*, Jae Hyun Joo, Kyung Sub Lee

Department of Materials Science and Engineering, Hanyang University, 17 Haengdang-dong, Seongdong-ku, Seoul 133-791, South Korea

Abstract

By optimized mechanical alloying (MA) and subsequent firing, spinel $LiMn_2O_4$ powders for 4 V lithium rechargeable batteries were prepared via direct reaction procedure, $Li_2O_2 + 2Mn_2O_3 \rightarrow 2LiMn_2O_4$. The resulted spinel oxide showed a maximum discharge capacity of 125 mAh/g at *C*/5 rate (29.6 mA/g), excellent capacity retention and rate capability with electrochemical cycling compared with the sample by the conventional solid-state reaction. Detailed powder properties such as mean particle size, lattice parameter, crystallite size and lattice strain were examined, and the chemical diffusion coefficients of lithium were determined. The improved electrode performances of MA powders originated mainly from the particle size refined to submicron size, reduced crystallite size and optimum lattice parameter, which enhanced the lithium transportation kinetics. In addition, it was found that the additional doping of iron was not effective to improve the cycleability of the sample by MA process.

Keywords: Spinel $LiMn_2O_4$; Mechanical alloying; Particle size; Lithium-ion battery

1. Introduction

The spinel $LiMn_2O_4$ has been widely studied as an alternative material to substitute layered $LiCoO_2$ cathode for 4 V lithium rechargeable batteries [1–3]. It is well known in this material that the electrochemical properties depend strongly on the synthesis method and conditions such as choice of starting materials, firing temperature and times, cooling rate and initial Li/Mn ratio [4,5]. Obviously, homogeneous composition and fine particle size are favorable for better cycling performances of the cathode materials. Several solution-based low-temperature synthetic processes such as sol–gel process, Pechini process and emulsion-drying process have been investigated to satisfy these criteria, and shown excellent electrochemical properties [6–8]. In commercial cell, nonetheless, the cathode material powders have been usually synthesized by the conventional solid-state reaction until now, because it is an easier and simple process. Consequently, from the well-established relationships between the structural parameters and electrochemical properties, the key point is how to manufacture the spinel by an easy and low-cost method.

Recently, the mechanical alloying (MA) method, which also referred to as mechanochemical synthesis, high energy ball milling, etc. has also been recommended as a useful technique to synthesize transition metal oxides for the lithium-ion battery [9–11]. In previous work, we have also showed that the spinel $LiMn_2O_4$ phase could be obtained by MA using the oxides of Li_2O_2 and Mn_2O_3 powders as the starting materials at room temperature [11]. Upon subsequent firing at 700 °C for only 2 h of MA powder, the well-crystallized spinel phase was obtained, which exhibited electrochemical performance comparable to those for earlier solution-based processes. In this study, the powder characteristics, rate capability and Fe doping effect in the sample prepared by MA were investigated and compared with those of a sample prepared by the conventional solid-state reaction in order to explain the reason for improvement in cycling behavior.

2. Experimental

The MA was carried out for 4 h using a shaker-type ball mill (SPEX8000 series) with a hardened steel vial set, and spinel $LiMn_2O_4$ powders were directly synthesized from Li_2O_2 and Mn_2O_3 as starting materials. Detailed MA conditions were described in the previous report [11]. To investigate the structural changes with firing temperature, the MA powders were fired at temperature ranging from 500 to 900 °C for 2 h under air (denote MA500, MA600, etc.).

* Corresponding author.
E-mail address: wtjeong@ihanyang.ac.kr (W.T. Jeong).

0378-7753/03/$ – see front matter © 2003 Elsevier Science B.V. All rights reserved.
doi:10.1016/S0378-7753(03)00229-5

For comparison, another $LiMn_2O_4$ sample was prepared by the conventional solid-state reaction. The simple mixture of the same starting materials, which were well mixed in an agate mortar, was fired at 650 °C for 12 h, and then 850 °C for 24 h under air (SM850). In addition, Fe-doped spinels ($x = 0.1, 0.2, 0.4$ in $LiFe_xMn_{2-x}O_4$) were also prepared by MA and solid-state reaction using a raw material of Fe_2O_3 as Fe source.

The crystal structures of the prepared samples were identified by X-ray diffractometer (Rigaku D-MAX 3000) using Cu Kα radiation. The lattice parameters were calculated by a least squares method using the internal Si reference. The composition of the samples was determined by inductively coupled plasma-atomic emission spectrometer (ICP-AES). The morphology and particle size distribution of prepared powders were examined by a scanning electron microscope (SEM) and a particle size analyzer (PSA).

Electrochemical cycle tests were performed using a two-electrode cell with a lithium metal foil as the negative electrode and a microporous polypropylene separator. The cathode consisted of 20 mg of active material, 12 wt.% of carbon black and 8 wt.% of polytetrafluoroethylene (PTFE). A dough-type cathode film of 1 cm^2 was pressed on a stainless Exmet screen and vacuum dried at least 12 h at 150 °C. The entire cell with an electrolyte of 1 M $LiPF_6$ in EC:DMC (1:1, v/v) mixture was assembled in an argon-filled dry box. The cut-off voltages were 3.3–4.3 V, and current density a *C*/5 rate (29.6 mA/g). The rate capability was investigated at various current density of *C*/*x* ($x = 1, 2, 5, 10, 20$). To determine the dependence of the lithium intercalation/de-intercalation rate expressed as chemical diffusion coefficient, D_{Li} in $Li_xMn_2O_4$, a galvanostatic intermittent titration technique (GITT) experiment was carried out using a three-electrode cell between 3.2 and 4.3 V at a constant current pulse of *C*/10 rate for 1800 s.

3. Results and discussion

With other optimized MA variables, the optimum MA time to produce a crystalline $LiMn_2O_4$ spinel phase was decided to 4 h in the previous work [11]. XRD patterns for the resulted as-MA powder (MA) and the structural evolution with increasing subsequent firing temperature are shown in Fig. 1. All samples revealed a well-defined cubic spinel structure with different crystallinity. During the MA process, the crystalline structure in powder particles is internally stressed and distorted as well as refined, resulting in line broadening of XRD peaks. In order to examine the variation of crystallite size and residual strains with subsequent firing after MA, the two components in the XRD peaks were separated by following equation using the Gaussian/Gaussian assumption [12,13]:

$$B^2 \cos^2\theta = 16e^2 \sin^2\theta + \frac{K^2\lambda^2}{L^2}$$

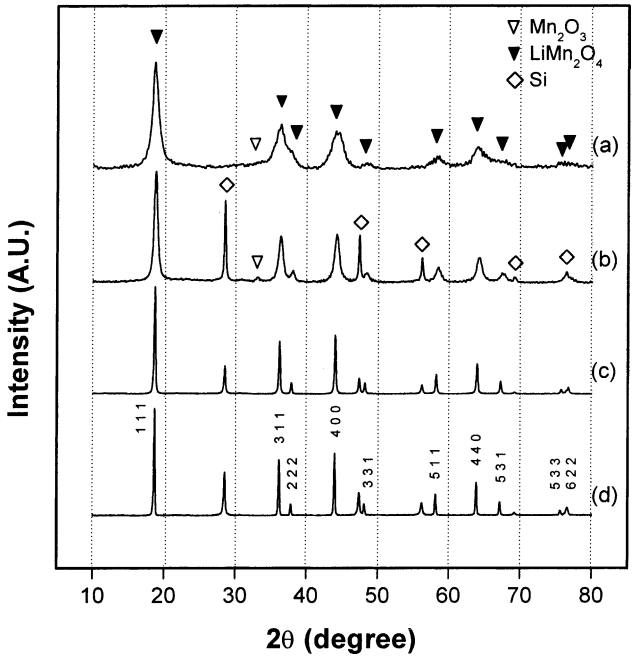

Fig. 1. XRD patterns for prepared $LiMn_2O_4$ samples: (a) MA (as-MA powder), (b) MA500, (c) MA700, (d) MA900.

where *B* is the integral breadth of the intensity peak on the 2θ scale in radians, *e* denotes maximum local strain of the crystalline structure, *K* is a near-unity constant related to the crystallite shape, λ wavelength of radiation (Cu Kα) and *L* is the mean crystallite size. Determined crystallite sizes and strains for the samples are plotted in Fig. 2, and the exact values are shown in Table 1 with other structural parameters. It can be seen that strains induced during the MA process were sufficiently released by firing at 700 °C for only 2 h. SM850 by the solid-state reaction had the lowest strains but larger crystallite size than MA900 due to prolonged reaction time. Table 1 also compares the mean particle size determined by PSA for MA, MA700 and SM850. On firing after MA, the particle size increased as expected, but the value was still in the range of submicron size. The other MA samples (MA500, MA600 and MA900) were also having submicron-sized particles from SEM observation. On the other hand, SM850 showed larger value than that for the starting materials. The mean particle size of starting material, Mn_2O_3 was 4.18 μm ranging from 0.3 to 10 μm. It is evident that the particle size distribution decreased by one order in MA700, but increased by one order in SM850 in spite of using the same starting materials.

Fig. 3 shows the result of electrochemical cycling at a current density of *C*/5 rate (29.6 mA/g) between 3.3 and 4.3 V for all samples except for as-MA (MA) sample. As can be seen, sample MA700 showed the largest initial discharge capacity and the best cycling performance. These features in the capacity with the firing temperature have been reported by many researchers [14,15]. Tarascon et al. suggested that the decrease in capacity with increasing temperature above

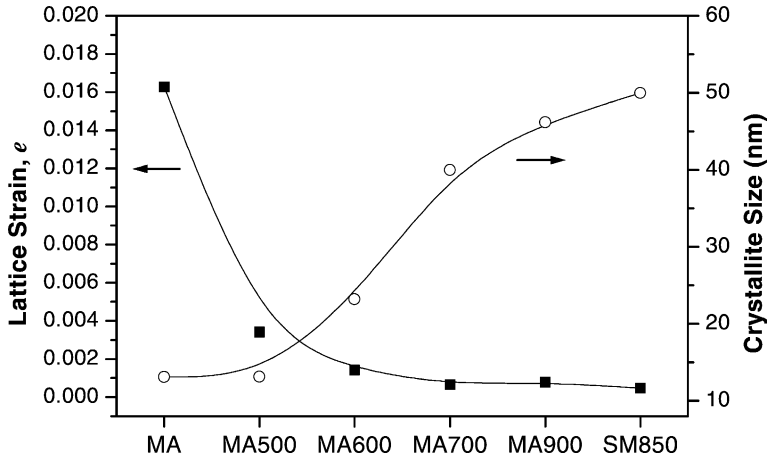

Fig. 2. Comparison of crystallite size and strain for mechanical-alloyed samples after firing at various temperature and a sample prepared by the conventional solid-state reaction (SM850).

Table 1
Synthesis conditions and structural parameters of prepared $LiMn_2O_4$ powders

Sample ID	Synthesis condition	Lattice parameter (Å)	Mean particle size (μm)[a]	Crystallite size (nm)	Strain, $\langle e \rangle$
MA	As-MA for 4 h	N/A[b]	0.34	13.08	1.63×10^{-2}
MA500	MA + 500 °C, 2 h	8.192	N/A	13.11	3.42×10^{-3}
MA600	MA + 600 °C, 2 h	8.209	N/A	23.19	1.42×10^{-3}
MA700	MA + 700 °C, 2 h	8.232	0.55	39.96	6.63×10^{-4}
MA900	MA + 900 °C, 2 h	8.253	N/A	46.17	7.93×10^{-4}
SM850	Solid-state reaction (650 °C, 12 h + 850 °C, 24 h)	8.245	15.8	49.98	4.73×10^{-4}

[a] Determined by particle size analyzer (PSA).
[b] N/A: not analyzed.

800 °C was due to changing grain size, not changing oxygen contents [15]. In addition, Amatucci et al. reported that the decrease in capacity and cycle life corresponded with an increase in lattice parameter that reached values greater than 8.23 Å at higher temperatures [16]. They set this value of lattice parameter as a necessary condition for the optimized electrochemical performance. In this study, the lattice parameter of 8.232 Å for MA700 which showed the best cycling performance was in good accordance with this criterion. Sample SM850 had an initial capacity close to that of MA700, but showed rapid cyclic fading faster than MA900. It is considered, therefore, that the improved electrode performances of MA samples originated mainly from the refined particle size, smaller crystallite size and lattice parameter.

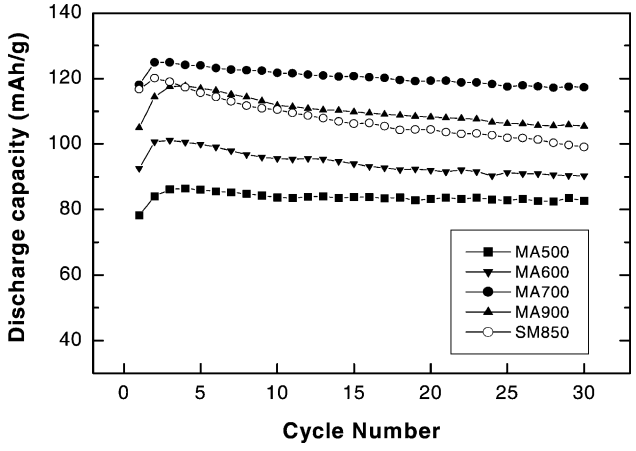

Fig. 3. Discharge capacity as a function of cycle number for prepared samples showing the effect of firing temperature. SM850 is a sample prepared by the conventional solid-state reaction.

Differential capacities for MA700 and SM850 with increasing the number of cycle are compared in Fig. 4. Both samples showed two peaks at about 4.0 and 4.1 V representing the two plateaus in charge–discharge curves. The higher-voltage peaks for SM850 were sharper than those for MA700 indicating the two-phase reaction, and diminishing rates of the peaks with cycling were faster in both higher and lower voltage peaks. This indicates that the structural stability of MA700 with electrochemical cycling was higher than that of SM850.

To evaluate the electrochemical performance as a function of applied current density, the second discharge curves for MA700 and SM850 at various discharge rates are compared in Fig. 5. It is apparent in both samples that discharge capacities and plateau potentials decreased with increasing discharge rate. However, MA700 exhibited smaller capacity decreases with increasing discharge rate, although two

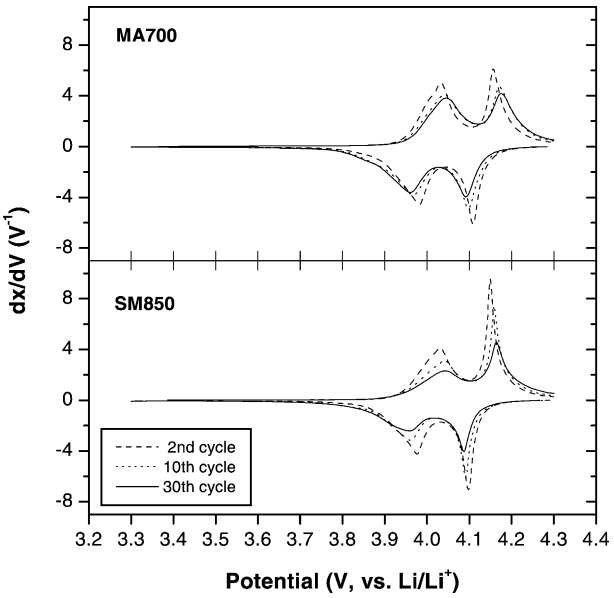

Fig. 4. Comparison of differential capacity curves as a function of cell potential with increasing the number of cycle for the samples MA700 and SM850.

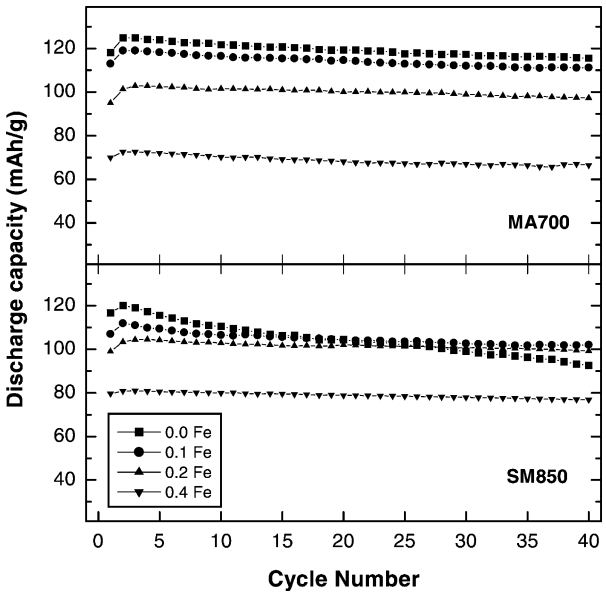

Fig. 6. Discharge capacity as a function of cycle number showing the effect of Fe doping ($x = 0$–0.4 in $LiFe_xMn_{2-x}O_4$) for the samples MA700 and SM850 cycled between 3.3 and 4.3 V at *C*/5 rate.

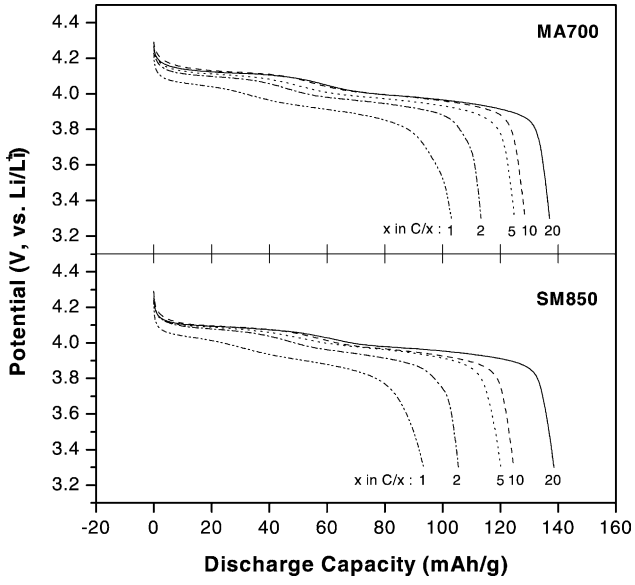

Fig. 5. Variation of discharge curves with various *C* rates for the samples MA700 and SM850.

samples showed about the same capacity around 138 mAh/g at very slow discharge rate of *C*/20 (7.4 mA/g). In order to elucidate the reason for this improved rate capability in MA700, the chemical diffusion coefficients of Li^+ ions (D_{Li}) were determined for the two samples by GITT method. The determined D_{Li} values for MA700 ($\sim 10^{-9}$ cm^2/s) were at least one order of magnitude larger than those for SM850 over entire Li composition. Consequently, it could be concluded that reduced crystallite size and particle size achieved by MA enhanced the Li transportation kinetics, and then led to improvement of rate capability.

Finally, the effects of Fe doping on electrode performance were investigated. During the MA process using steel balls and vial, a certain degree of Fe contamination was inevitable. In this study, Fe contents in MA samples measured by ICP analysis were about $x = 0.07$ in $LiFe_xMn_{2-x}O_4$ form. In general, Mn substitution with some metal ions decreases initial discharge capacity and improves electrochemical cycleability of spinel $LiMn_2O_4$ by increasing the average Mn valence. Therefore, in order to separate the Fe doping effect in improved electrochemical performance of MA700 and compare with the doping effect in SM850, Fe-doped ($x = 0.1$, 0.2, 0.4 in $LiFe_xMn_{2-x}O_4$) samples were prepared by MA and solid-state reaction. Fig. 6 compares the results of electrochemical cycling test for the prepared samples. In both samples, initial discharge capacities were decreased in a same manner with increasing Fe doping up to $x = 0.4$. However, cycleability was significantly improved in SM850, whereas not in MA700 with Fe doping. This means that the improved electrode performance of MA700 was mainly caused by the characteristics of MA powder. Furthermore, it is considered that $LiMn_2O_4$ samples prepared by optimized MA process did not require the doping of transition metal in order to improve the cycling performance.

4. Conclusions

Using the starting materials of Li_2O_2 and Mn_2O_3, spinel $LiMn_2O_4$ powder was directly synthesized by MA. The as-MA powder was composed of submicron-sized particles with significant lattice strains and poor crystallinity. Upon firing at 700 °C for only 2 h (MA700), the strains were sufficiently released maintaining submicron-sized particles,

and well-ordered spinel structure with a lattice parameter of 8.232 Å could be obtained. With this microstructural features, MA700 exhibited a good electrochemical cycling behavior and rate capability compared with SM850 prepared by the solid-state reaction, showing enhanced Li transportation kinetics. In addition, it was found that the additional doping of iron was not effective to improve the cyceability of the samples by MA process. Consequently, it is reconfirmed that the MA process is the one of promising methods to synthesize the spinel $LiMn_2O_4$ oxides for lithium rechargeable batteries.

Acknowledgements

This work was supported by the research fund of Hanyang University (HY-2000).

References

[1] T. Ohzuku, M. Kitagawa, T. Hirai, J. Electrochem. Soc. 137 (1990) 769.
[2] R.J. Gummow, A. de Kock, M.M. Thackeray, Solid State Ionics 69 (1994) 59.
[3] X.Q. Yang, X. Sun, M. Balasubramanian, J. McBreen, Y. Xia, T. Sakai, M. Yoshio, Electrochem. Solid-State Lett. 4 (2001) A117.
[4] P. Endres, B. Fuchs, S.K. Sack, K. Brandt, G.F. Becker, H.W. Praas, Solid State Ionics 89 (1996) 221.
[5] Y. Xia, T. Sakai, T. Fujieda, X.Q. Yang, X. Sun, Z.F. Ma, J. McBreen, M. Yoshio, J. Electrochem. Soc. 148 (2001) A723.
[6] S.H. Park, K.S. Park, Y.K. Sun, K.S. Nahm, J. Electrochem. Soc. 147 (2000) 2116.
[7] W. Liu, G.C. Farrington, F. Chaput, B. Dunn, J. Electrochem. Soc. 143 (1996) 879.
[8] C.H. Lu, S.W. Lin, J. Power Sources 93 (2001) 14.
[9] N.V. Kosova, N.F. Uvarov, E.T. Devyatkina, E.G. Avvakumov, Solid State Ionics 135 (2000) 107.
[10] W.T. Jeong, K.S. Lee, J. Power Sources 104 (2002) 195.
[11] W.T. Jeong, J.H. Loo, K.S. Lee, J. Alloys Comp., in press.
[12] L. Hernán, J. Morales, L. Sánchez, J. Santos, Solid State Ionics 104 (1997) 205.
[13] H.P. Klug, L.E. Alexander, X-ray Diffraction Procedure for Polycrystalline and Amorphous Materials, Wiley, New York, 1974, p. 665.
[14] T. Nakamura, A. Kajiyama, Solid State Ionics 124 (1999) 45.
[15] J.M. Tarascon, E. Wang, F.K. Shokoohi, W.R. McKinnon, S. Colson, J. Electrochem. Soc. 138 (1991) 2859.
[16] G.G. Amatucci, C.N. Schmutz, A. Blyr, C. Sigala, A.S. Gozdz, D. Larcher, J.M. Tarascon, J. Power Sources 69 (1997) 11.